NASA/TM—2013-216569 AIAA–2013–3982

# Warm Pressurant Gas Effects on the Liquid Hydrogen Bubble Point

*Jason W. Hartwig, John B. McQuillen, and David J. Chato*
*Glenn Research Center, Cleveland, Ohio*

September 2013

# NASA STI Program . . . in Profile

Since its founding, NASA has been dedicated to the advancement of aeronautics and space science. The NASA Scientific and Technical Information (STI) program plays a key part in helping NASA maintain this important role.

The NASA STI Program operates under the auspices of the Agency Chief Information Officer. It collects, organizes, provides for archiving, and disseminates NASA's STI. The NASA STI program provides access to the NASA Aeronautics and Space Database and its public interface, the NASA Technical Reports Server, thus providing one of the largest collections of aeronautical and space science STI in the world. Results are published in both non-NASA channels and by NASA in the NASA STI Report Series, which includes the following report types:

- TECHNICAL PUBLICATION. Reports of completed research or a major significant phase of research that present the results of NASA programs and include extensive data or theoretical analysis. Includes compilations of significant scientific and technical data and information deemed to be of continuing reference value. NASA counterpart of peer-reviewed formal professional papers but has less stringent limitations on manuscript length and extent of graphic presentations.

- TECHNICAL MEMORANDUM. Scientific and technical findings that are preliminary or of specialized interest, e.g., quick release reports, working papers, and bibliographies that contain minimal annotation. Does not contain extensive analysis.

- CONTRACTOR REPORT. Scientific and technical findings by NASA-sponsored contractors and grantees.

- CONFERENCE PUBLICATION. Collected papers from scientific and technical conferences, symposia, seminars, or other meetings sponsored or cosponsored by NASA.

- SPECIAL PUBLICATION. Scientific, technical, or historical information from NASA programs, projects, and missions, often concerned with subjects having substantial public interest.

- TECHNICAL TRANSLATION. English-language translations of foreign scientific and technical material pertinent to NASA's mission.

Specialized services also include creating custom thesauri, building customized databases, organizing and publishing research results.

For more information about the NASA STI program, see the following:

- Access the NASA STI program home page at *http://www.sti.nasa.gov*

- E-mail your question to *help@sti.nasa.gov*

- Fax your question to the NASA STI Information Desk at 443–757–5803

- Phone the NASA STI Information Desk at 443–757–5802

- Write to:
  STI Information Desk
  NASA Center for AeroSpace Information
  7115 Standard Drive
  Hanover, MD 21076–1320

NASA/TM—2013-216569 AIAA–2013–3982

# Warm Pressurant Gas Effects on the Liquid Hydrogen Bubble Point

*Jason W. Hartwig, John B. McQuillen, and David J. Chato*
*Glenn Research Center, Cleveland, Ohio*

Prepared for the
49th Joint Propulsion Conference and Exhibit
cosponsored by the AIAA, ASME, SAE, and ASEE
San Jose, California, July 14–17, 2013

National Aeronautics and
Space Administration

Glenn Research Center
Cleveland, Ohio 44135

September 2013

## Acknowledgments

This work was funded by the Cryogenic Propellant Storage and Transfer Project under the Office of the Chief Technologist at NASA. The authors would like to thank the operations team and research support staff at CCL-7 for their assistance during planning, design, and testing phases.

*Level of Review*: This material has been technically reviewed by technical management.

Available from

NASA Center for Aerospace Information
7115 Standard Drive
Hanover, MD 21076–1320

National Technical Information Service
5301 Shawnee Road
Alexandria, VA 22312

Available electronically at http://www.sti.nasa.gov

# Warm Pressurant Gas Effects on the Liquid Hydrogen Bubble Point

Jason W. Hartwig, John B. McQuillen, and David J. Chato
National Aeronautics and Space Administration
Glenn Research Center
Cleveland, Ohio 44135

## Abstract

This paper presents experimental results for the liquid hydrogen bubble point tests using warm pressurant gases conducted at the Cryogenic Components Cell 7 facility at the NASA Glenn Research Center in Cleveland, Ohio. The purpose of the test series was to determine the effect of elevating the temperature of the pressurant gas on the performance of a liquid acquisition device. Three fine mesh screen samples (325×2300, 450×2750, 510×3600) were tested in liquid hydrogen using cold and warm noncondensible (gaseous helium) and condensable (gaseous hydrogen) pressurization schemes. Gases were conditioned from 0 to 90 K above the liquid temperature. Results clearly indicate a degradation in bubble point pressure using warm gas, with a greater reduction in performance using condensable over noncondensible pressurization. Degradation in the bubble point pressure is inversely proportional to screen porosity, as the coarsest mesh demonstrated the highest degradation. Results here have implication on both pressurization and LAD system design for all future cryogenic propulsion systems. A detailed review of historical heated gas tests is also presented for comparison to current results.

### Nomenclature

| | |
|---|---|
| $d_{shute}$ | diameter of the shute wire (μm) |
| $d_{warp}$ | diameter of the warp wire (μm) |
| $g$ | gravitational acceleration (m/s$^2$) |
| $l_s$ | distance between consecutive shute wires (μm) |
| $n_{shute}$ | number of shute wires per inch of screen (1/m) |
| $n_{warp}$ | number of warp wires per inch of screen (1/m) |
| $t$ | screen thickness (μm) |
| $D_p$ | effective pore diameter (μm) |
| *HEX* | heat exchanger |
| *LL* | liquid level above LAD screen (m) |
| *PCA* | pressure control |
| γ | Surface tension (mN/m) |
| ε | porosity |
| $\rho_{LH2}$ | liquid hydrogen density (kg/m$^3$) |
| $\theta_c$ | contact angle (degrees) |
| $\Delta P_{BP}$ | bubble point pressure (Pa) |
| $\Delta T$ | temperature difference between liquid and pressurant gas (K) |

## 1.0 Introduction

NASA maintains a strong desire to develop technology to enable long duration robotic and human space missions beyond low Earth orbit (LEO). Future destinations include Earth-Moon Lagrange points, near-Earth objects (NEOs) such as asteroids, and eventually surface missions to the Moon, Mars, and beyond. The development of new and existing propulsion capabilities to send robot and human afar is necessary for the exploration and study of these locations of interest. Due to significant increase in propulsion system performance compared to storable propellants (fluids that exist as liquids at room temperature), the advancement of cryogenic fluid propulsion systems remains at the forefront of NASA's technology development program.

Liquid oxygen/liquid hydrogen (LOX/LH$_2$) remains the top propellant combination owing to both an unmatched level of performance relative to other combinations, and due to proven flight heritage over the past 40 years in launch systems such as the Saturn V-S4, S4B, S2, Shuttle Space Transportation System (STS), short duration upper stages (J2), and potential LEO fuel depots (Ref. 1). However there are challenging aspects when working with cryogenic propellants due to a low normal boiling point (NBP), low surface tension, and low viscosity. Cryogenic propellants are particularly susceptible to parasitic heat leak, which will make in-space storage and transfer a challenge.

## 2.0 Screen Channel Liquid Acquisition Devices

Technology development for LOX/LH$_2$ cryogenic propulsion systems begins upstream in the propellant tanks. Conceivably, there are two applications for in-space cryogenic liquid transfer, from the storage tank to the transfer line to an engine, or from a fuel depot to a receiver tank. All cryogenic propulsion engines require vapor free liquid to be delivered to the injectors. Receiver depot tanks will also require very high liquid fill fractions due to the projected cost of launching and storing propellant in LEO in fuel depots. Single phase liquid acquisition in Earth's 1-g environment is straightforward, since gravity drives the heavier liquid to the bottom and lighter vapor to the top of the propellant tank. In microgravity conditions of LEO however, any one of a number of special propellant management devices (PMDs) may be required to draw

sufficient liquid to the tank outlet in varying thermal and gravitational environments. One type of PMD, a screen channel liquid acquisition device (LAD), relies on capillary flow and surface tension forces to acquire and maintain communication between the bulk liquid and tank outlet at all times. As shown in Figure 1, screen channel LADs follow the contours of the tank walls. The side that faces the wall is covered with a fine mesh screen that acts to wick liquid into the channel and also serve as a barrier to vapor ingestion during outflow if vapor is in contact with the screen.

Screen channel LADs are characterized by the screen weave and mesh type, which refers to the number of wires per inch of material and type of pattern used during manufacture. For example, the 510×3600 screen is a Dutch Twill mesh with 510 warp wires and 3600 shute wires per square inch of material as shown in Figure 2. Each shute wire passes under two warp wires before going over the next warp wire, which creates a tortuous path to vapor ingestion. The screen selection is dictated by specific mission requirements, which include gravitational and thermal environments, and flow rate demands. Finer mesh screens are favorable for $LH_2$ systems to counter the low surface tension.

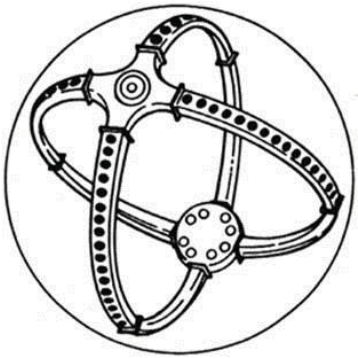

Figure 1.—Full Communication Screen Channel LAD

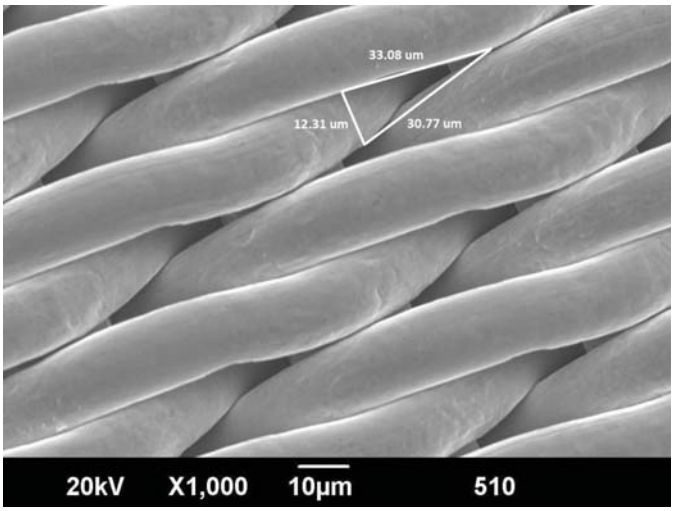


Figure 2.—Scanning Electron Microscopy Image of a 510x3600 Screen

Screen channel LADs have proven flight heritage in storable propulsion systems such as the STS Reaction Control System (RCS) and Orbital Maneuvering System (OMS) (Refs. 2 to 5), and in cryogenic liquid helium (LHe) (Ref. 6), but have not been used with $LH_2$ or LOX in low gravity. For flight systems, screen channel LADs are divided into two regimes (Refs. 7 and 8). Start baskets or traps are small LADs that can be used in systems that experience large accelerations and large flow rates under short durations. Meanwhile full communication devices such as those depicted in Figure 1 are used in systems with small accelerations and small flow rates under longer durations.

## 3.0 Pressurization System/LAD System Interaction

Besides LADs, there are several other subsystems required for cryogenic fluid management (CFM) inside a flight propellant tank. Passive thermal control is maintained through multilayer insulation (MLI) systems while active thermal control is achieved through the use of cryocooler heat exchangers. Thermodynamic vent systems are used to control pressure inside the tank. Mass gauging systems are used to gauge propellant in the varying gravitational levels of LEO. Pressurization systems, which include the gas bottles, pressure control, and heat exchanger, are used to pressurize and drain the tank during expulsion. Finally, LADs are used to separate liquid and vapor inside a propellant tank and ensure transfer of vapor free liquid from the tank into the outlet line.

During spaceflight, there are two primary sources of heat leak into the tank as indicated by the red arrows in Figure 3; one associated with storage and one with transfer of the propellant. Radiation and conduction heat leak enters the tank through the support struts, fill, vent, and instrumentation penetrations. Mitigation strategies to reduce heat leak are straightforward; passive thermal control is used to reduce heat leak by using thick MLI blankets, composite struts, and optimizing the MLI layer density, while active thermal control techniques use a heat exchanger to reduce or eliminate propellant boil off. A second source of heat leak into the tank is from warm pressurant gas contacting the cold liquid propellant during liquid transfer. Mitigation strategies here are complicated. From a systems level standpoint, it is highly desirable to use warm gas as a pressurant because less mass is required to thermally condition the gas to tank conditions. From the LAD subsystem standpoint however, it is desirable to use cold gas because LADs are surface tension driven devices, and colder temperatures result in better performance.

During spaceflight, the pressurant gas typically assumes the environmental temperature, which is warmer than the saturation temperature for cryogenic propellants at atmospheric pressure. Even if the pressurant tank bottle is thermally linked to the propellant tank, the pressurant gas temperature will still

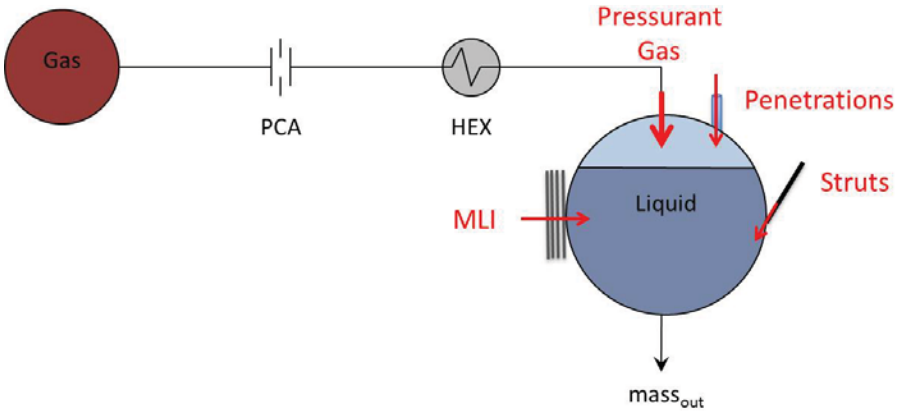


Figure 3.—Sources of Heat Leak into a Cryogenic Propellant Tank

be warmer than the liquid temperature. As will be shown later, warm pressurant will always decrease the surface tension of the cryogen, consequently, degrading the LAD performance. Clearly an optimal design point between the pressurization and LAD subsystems exists for each mission. Tests are also warranted to quantify the effect of heat absorption into the liquid on the LAD performance.

In regard to the pressurization subsystem, there are two ways to pressurize a cryogenic propellant tank during liquid transfer. Autogenous pressurization utilizes the liquid's own vapor to pressurize while noncondensible pressurization employs a gas that will not condense into the liquid during pressurization. From a systems level standpoint, autogenous pressurization is more attractive due to overall lower system mass and potential reduced system complexity. However, this system may require heaters or pressure building circuits to maintain sufficient liquid flow rates. In addition, autogenous pressurization complicates liquid transfer due to added heat and mass transport across the LAD screen during outflow, which can prematurely warm the liquid and potentially cause the LAD to break down early. Therefore autogenous pressurization may be insufficient to sustain high outflow rates for prolonged periods of time. Meanwhile, pressurization with a noncondensible gas, such as helium, results in less heat and mass transfer at the LAD screen during outflow and also incurs less dissolution in all major cryogenic propellants (Ref. 9). Helium pressurization is likely sufficient to sustain all anticipated outflow rates (Ref. 10). However, noncondensible pressurization requires the use of onboard gas bottles as shown in Figure 3, which increases overall system mass. In addition, GHe pressurization may be more expensive than autogenous pressurization because of the increasing cost of gaseous helium supplies. In a long duration depot mission GHe is a consumable resource which limits mission duration. Being able to generate pressurant (autogenous) eliminates issues associated with resupply of GHe. Additionally GHe addition affects saturation pressure in the tank.

## 4.0 The Bubble Point Pressure

A screen channel LAD is said to have failed when vapor or gas is ingested into the channel, since the purpose of the LAD is to prevent gas ingestion into the channel. This failure or breakdown point is called the bubble point of the LAD screen. The bubble point is defined as the differential pressure across a LAD screen pore that overcomes the surface tension forces at that pore. Bubble point pressure, $\Delta P_{BP}$, is proportional to the surface tension of the liquid and inversely proportional to the effective screen pore diameter, as derived in (Refs. 11 and 12) and shown in Equation (1):

$$\Delta P_{BP} = \frac{4\gamma \cos\theta_C}{D_P(T)} \tag{1}$$

where $\gamma$ is the surface tension of the fluid (mN/m), $\theta_C$ is the contact angle, and $D_P$ is the effective pore diameter (μm). Vapor bubbles that penetrate into the channel may be condensed if conditions within the LAD are subcooled. However, helium bubbles that penetrate into the channel can only dissolve into the liquid, which is a very slow process, and could potentially cause engine instability.

The effective pore diameter is most readily determined through room temperature bubble point tests in a reference fluid such as isopropyl alcohol (IPA), which provides a good calibration range for low surface tension cryogenic liquids. Hartwig et al. (2013) (Ref. 13) showed that the pore diameter is temperature dependent, and derived a simple pore diameter model to account for screen pore diameter shrinkage at colder temperatures to account for differences in bubble points for the same screen that could not be attributed to the fluid surface tension. Measurement of pore diameters using scanning electron microscopy (SEM) imaging has proven unreliable (Refs. 14 and 15). In addition, there are inconsistencies about performance based on wire counts. For example, the 450×2750 mesh outperforms both the 325×2300 and 510×3600 meshes in room

temperature and cryogenic liquids (Refs. 14 and 16). However, the performance of the coarser 325 mesh surpasses the performance of the 510 mesh in room temperature liquids, but the opposite occurs in liquid nitrogen ($LN_2$) and $LH_2$. Note that Equation (1) does not differentiate for pressurization gases. Previous experimental programs using cryogenic liquids, $LH_2$, LOX, and liquid methane ($LCH_4$) have demonstrated better performance when pressurizing with a noncondensible pressurant gas like gaseous helium (GHe) versus pressurization with an condensable gas such as gaseous hydrogen ($GH_2$) (Refs. 14, 17 to 20).

Screen channel LADS have flight heritage with storable propellants where heat transfer effects are not as severe as they are for cryogenic propellants. Before these LADs can be routinely used in cryogenic propulsion systems, the effects of undesirable heat on the LAD must be fully quantified. This environmental parasitic heat leak into the tank or heat input from warm pressurant gas may adversely affect LAD performance by vaporizing the liquid and drying out the LAD screen. The static bubble point pressure is the upper limit on the total allowable pressure loss in a LAD system and therefore serves as the primary performance parameter for characterizing a screen channel LAD.

## 5.0 Test Objectives

Issues that arise in $LH_2$ cryogenic fluid management have been addressed through a battery of ground tests between FY11 to FY13 as part of the Cryogenic Propellant Storage and Transfer (CPST) technology maturation plan for the CPST Technology Demonstration Mission (TDM). Previous work has addressed the effect of varying the screen mesh, liquid, liquid temperature and pressure, and type of pressurization gas on the liquid hydrogen bubble point. The purpose of this work was to examine the effect of warm pressurant gas on the bubble point of screen channel liquid acquisition devices. The goal is to give mission designers direct insight into the combined LAD and pressurization subsystem performance and design for future cryogenic engines and cryogenic fuel depots.

## 6.0 Previously Reported Experiments

The easiest and most straightforward method to characterize the limits for a screen channel LAD is to measure the bubble point of a small screen sample. The method using an inverted bubble point (IBP), with liquid on top and vapor or gas on the bottom, is preferable over the non-inverted bubble point (NIBP) method for the following reasons: It is easier to control liquid head pressure on the submerged LAD screen sample, it is easier to deduce breakthrough pressures, and bubbles that break through the screen naturally rise away from the screen during breakthrough. A third method for testing LAD performance involves flowing liquid through a complete LAD channel assembly until the screen breaks down and vapor is ingested into the channel. Static IBP or NIBP tests are preferred over dynamic inverted outflow tests because IO test results can vary based on how the tank was pressurized, how the gas impinges on the screen (ex. parallel vs. perpendicular to screen face), and due to nonuniform pressurization gas temperature gradients which may develop during outflow. A fourth method for testing LAD performance is similar to the bubble point testing and involves immersing the entire screen element in liquid, draining the liquid, and pressuring the element with gas until bubble breakthrough. This method is used to test start baskets and traps, which are used for holding small amounts of liquid within the tank for engine restart.

A rigorous review of the literature revealed a total of 10 relevant studies of warm pressurant gas effects on LAD performance. LAD performance is affected by the surface tension, and, thus temperature. Therefore to make meaningful comparisons, historical results are organized by propellant type (function of saturation temperature), and then by screen type. A brief overview of historical results is presented chronologically. Results are shown in Figure 4 to Figure 9. To allow comparison between the four previously described methods, a normalized bubble point ratio is defined:

$$\frac{\Delta P_{BP}\left(\Delta T\right)}{\Delta P_{BP}\left(\Delta T = 0\right)} \tag{2}$$

where $\Delta T$ is the temperature difference between liquid propellant and pressurant gas. Therefore the denominator is the normal breakdown value for equal gas and liquid temperatures, and the numerator is the breakdown value when the gas is sufficiently heated above the liquid temperature (i.e., the temperature difference across the screen). The normalized ratio is plotted as a function of the temperature difference across the screen.

Castle and Klevatt (Ref. 21) first attempted to quantify the effect of heated pressurant on screen channel LAD performance. Using a standard NIBP configuration, they reported static bubble point tests conducted in $LN_2$ using gaseous nitrogen ($GN_2$) for six different screen samples. $GN_2$ was heated electrically and forced downward on the LAD screen using a fan in an attempt to eliminate natural convection in favor of forced convection. As shown in Figure 8, for a $\Delta T$ = 50 K across the screen, there was no degradation in performance for any screen mesh. Only the 250x600 mesh screen showed a percent degradation in performance at a $\Delta T$ = 250 K.

Burge and Blackmon (Ref. 7) reported heated gas $LH_2$ bubble points using a similar NIBP configuration as Castle and Klevatt for three different meshes using $GH_2$ as a pressurant, as shown in Figure 4. A fan forced hot $GH_2$ down on the screen, but no attempt was made to eliminate natural convection. Results show performance degradation for all of the screens tested, with the finer 250×1370 mesh performing

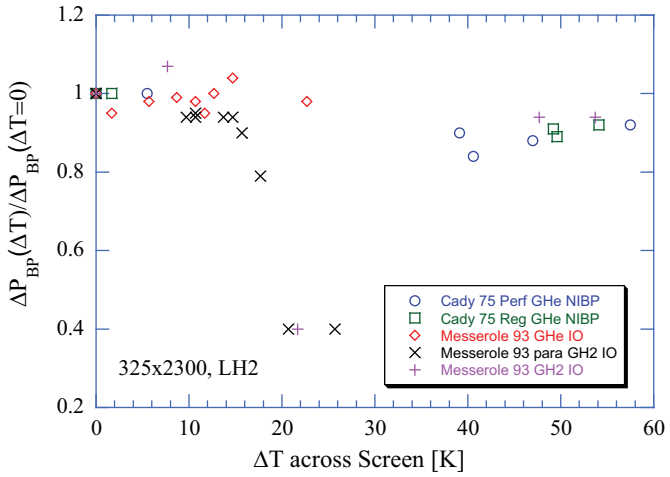


Figure 4.—Heated Pressurant Gas LAD Performance Data for a 325x2300 Screen in $LH_2$

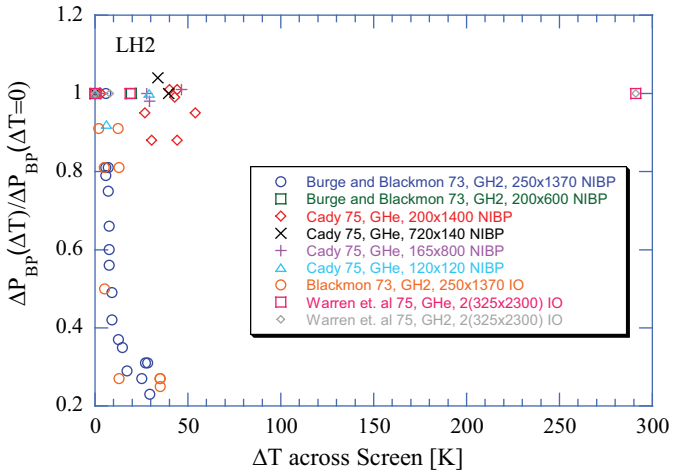


Figure 5.—Remaining Heated Pressurant Gas Data in Liquid Hydrogen

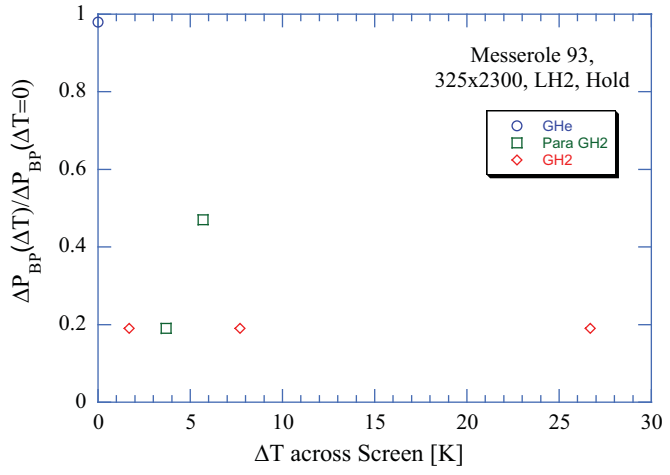


Figure 6.—Inverted $LH_2$ Outflow Hold Tests for a 325x2300 Mesh from (Ref. 29) Using Heated Pressurant Gas

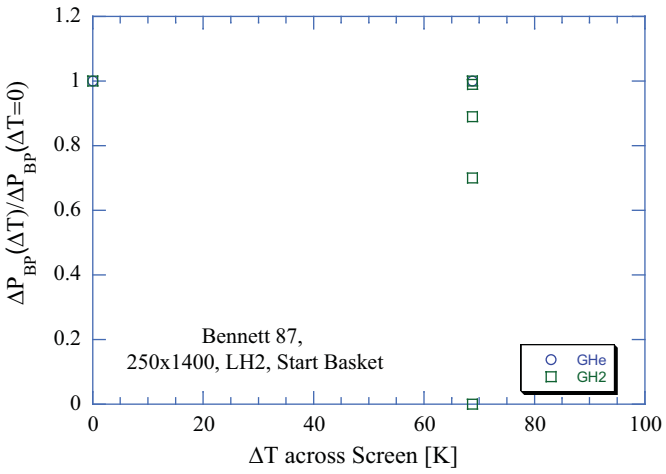


Figure 7.—Warm Pressurant Gas Start Basket LAD Performance Tests in $LH_2$ from (Ref. 28)

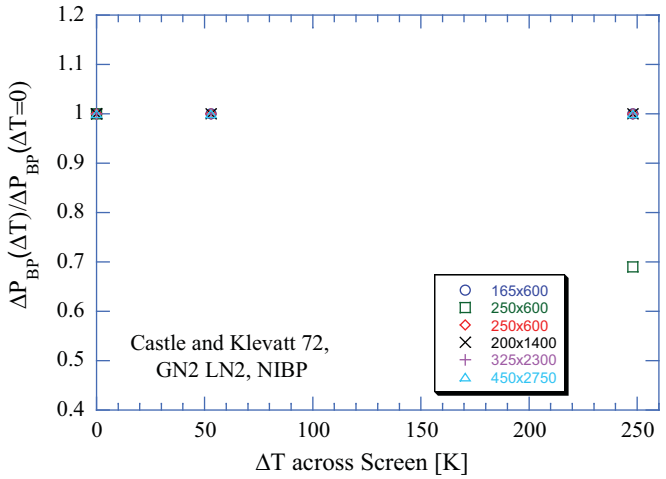


Figure 8.—Heated Non-inverted Bubble Point Data in Liquid Nitrogen

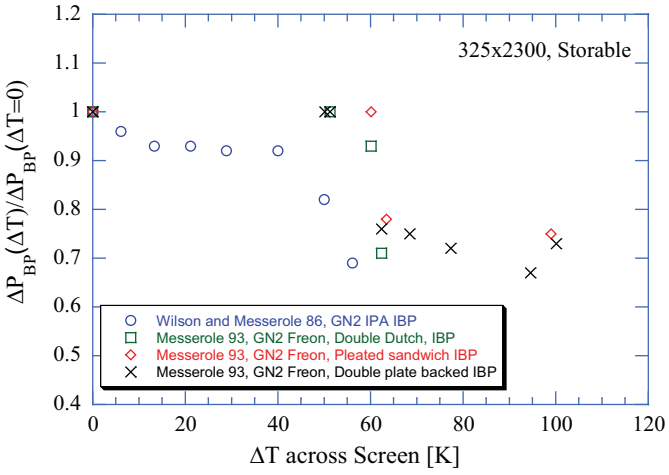


Figure 9.—Warm Pressurant Gas LAD Performance Data for a 325x2300 Screen in IPA and Freon

much worse than the coarser 200×600 mesh. The 250 mesh degraded to 30 percent of the cold gas breakdown point. Burge and Blackmon (Ref. 7) also reported premature breakdown for a 200×1400 mesh with $GH_2/LH_2$ of 50 percent but did not report the gas temperature at breakdown. Due to the existence of both natural and forced convection, the screen likely broke down prematurely for all these tests. In addition, results are complicated by the fact that the liquid may have been subcooled relative to the pressurant gas temperature.

Paynter et al. (Ref. 22) then conducted the first set of IO tests in $LH_2$ using both GHe and $GH_2$. Test conditions were not reported, but Paynter reported no premature breakdown with warm gas under steady continuous outflow conditions, but premature breakdown for stepped or ramped expulsions. Blackmon (Ref. 23) later conducted IO tests for a 250×1370 mesh in $LH_2$ using warm GHe and $GH_2$. Results from Figure 4 indicate a degradation in LAD performance as low as 75 percent at a $\Delta T$ = 35 K. Building on Paynter's tests, Warren (Ref. 24) and Warren et al. (Ref. 25) report IO data using two layers of 325x2300 screen mesh in $LH_2$ using both warm GHe and $GH_2$. Neither saw premature LAD breakdown for continuous or stepped expulsion for a $\Delta T$ = 19 to 291 K as shown in Figure 4.

Cady (Ref. 26) reported NIBP test data for a standard 325×2300 screen, a pleated 325×2300, a stainless steel (SS) and aluminum (Al) 200×1400 screen, a 720×140, 165×800, and a SS and Al 120×120 screen in $LH_2$ using warm GHe. Results are plotted in Figure 4 and Figure 5. As shown, there is degradation in heated bubble point values for all meshes tested, with the largest reduction in performance for the 200×1400 screen. On average there was greater than 10 percent reduction in bubble point for temperature differences between gas and liquid as high as $\Delta T$ = 55 K. When compared to other heated gas 325×2300 LAD data in Figure 4, the data follows the general trend. Cady saw no difference between pleated and unpleated screen performance and saw no difference in performance between SS and Al screens. Examination of the test apparatus however showed that there was a direct view factor between heating source and screen. Therefore results here are complicated by the fact that heat was being conducted into the pressurant gas and also into the screen itself, which may have caused early breakdown. In addition, it is difficult to compare results from this NIBP configuration where only natural convection was present with those from (Ref. 21) where forced convection is dominate with (Ref. 7) where forced and natural convection were present.

Wilson and Messerole (Ref. 27) report the first known heated pressurant gas LAD performance data using the IBP test configuration for a 325×2300 screen using $GN_2$ in IPA. As shown in Figure 9, they reported a reduction in performance of 69 percent of the cold gas bubble point at a $\Delta T$ = 56 K. But this data may also be corrupted due to the presence of a direct view factor between heat source and screen; the screen may have broken down early due to additional radiation heat transfer.

Bennett (Ref. 28) tested the liquid retention capability of a 34 cm tall 250×1400 start basket with a 200×1400 window in $LH_2$ using both noncondensible and autogenous pressurization schemes. Here the basket was submerged in liquid into a dewar, the liquid level lowered below the basket, and warm pressurant gas was introduced until the basket ingested vapor. With GHe pressurant, no degradation in performance was noted, even when the LAD was subjected to GHe 70 K above the liquid temperature as shown in Figure 7. Using $GH_2$ pressurant however, results were not repeatable as the start basket broke down at a height of 0, 70, and 90 percent of the cold gas height.

The most recent investigation was conducted by Messerole and Jones (Ref. 29) for a 325×2300 screen in $LH_2$ using both GHe and $GH_2$ using an IO test configuration and using $GN_2$ in Freon in an IBP configuration. In the IBP case, $GN_2$ was heated inside a cup with a heating element that was blocked from the screen to prevent stray radiation between heat source and screen. Gas was heated en route to the screen, which was submerged in Freon. A 325×2300 double-Dutch perforated plate, double plate backed 325×2300, and a pleated screen sandwich (325×2300, 25×25, 325×2300) were tested. As shown in Figure 9, the double-Dutch and double pleated samples did not improve screen retention, as bubble point pressure degraded to 57 and 67 percent of the cold gas values, respectively, for $\Delta T$ = 83 and 100 K, respectively. The onset of degradation did not occur until the gas temperature had risen 40 K above that of the liquid. The pleated sandwich also did not improve screen retention over a single 325×2300 screen, as warm gas bubble point degraded to 75 percent at a $\Delta T$ = 99 K.

Messerole and Jones (Ref. 29) also tested a 325×2300 perforated plate sample in $LH_2$ in a modified version of the test apparatus used in the Freon tests, in the IO configuration, and also in hold tests where liquid outflow was stopped for a period of time to allow sufficient residence time of the warm gas inside the dewar that held the LAD channel. IO test results using GHe, para-$GH_2$, and normal $GH_2$ are plotted in Figure 4 and hold tests are plotted in Figure 6. The trends are obvious; for GHe, for a $\Delta T$ as high as 62 K, there is insignificant degradation (less than 5 percent reduction in performance). For hold tests with warm GHe, there is no change in performance. For normal $GH_2$ pressurization, only a 6 percent reduction in performance is reported for a $\Delta T$ = 54 K during continuous expulsion tests; for stepped expulsion tests, the LAD broke down at a height of 19 percent of the cold gas height when the $GH_2$ was only 5 K above the liquid temperature. For para-$GH_2$ outflow tests, the LAD broke down at a height of 40 percent of the cold gas value at a $\Delta T$ = 26 K; for hold tests, the LAD broke down at a height of 19 percent of the cold gas height for a $\Delta T$ = 6 K.

Although trends from (Ref. 29) are fairly obvious, in that GHe performed much better than $GH_2$ for both IBP and IO test configurations, the results are not repeatable and are complicated by the following reasons. First, the LAD itself was not sized properly. The hydrostatic head pressure inside the LAD when the LAD was completely exposed to gas was never enough to overcome the static bubble point pressure. As a result of the poorly sized LAD, a flow restriction orifice was used on the $LH_2$ inflow to help build up additional pressure differential. LAD breakdown was actually induced through the use of this flow restriction at the bottom of the tank by ramping the ullage pressure while still flowing through the flow restriction. The liquid level always dropped below the bottom of the LAD screen and breakdown only occurred when ramping the ullage pressure. It is unclear what the flow rate was during this pressurization event; this is an indirect (and not direct) way to break the channel down. Second, warm gas was always injected at a temperature much greater than the actual temperature of the gas at the screen at breakthrough. Without direct measure of the temperature at the screen, it is unclear what the actual gas temperature was at the screen at breakdown. Third, for IO tests, a curved LAD was used, which only serves to complicate interpretation of results due to nonuniform flow through screen pressure losses. Fourth, while GHe and para-H2 tests were fairly repeatable, there is quite a large discrepancy between para-$GH_2$ and normal $GH_2$ results, despite the fact that there is only a 1 to 2 percent increase in surface tension for para over normal hydrogen gas.

In summary, past inverted outflow tests are not ideal for assessing the fundamental effect of warm pressurant gas on LAD performance due to complexities in reducing the data, in controlling pressurant gas flow, and in controlling uniformity of the gas temperature. Dynamic IO tests are more flight representative than the simple static screen sample tests because the IO tests simulate 1-g outflow through a LAD channel from a larger propellant tank. However, for IO outflow tests, it is extremely difficult to control the location and direction of pressurization and also the uniformity of the temperature of the warm gas inside the tank relative to the LAD; even small changes in the direction or temperature of the gas can cause noticeable differences in the breakdown height of the channel as is shown in the historical data. The NIBP configuration is also not preferred due to complexities in controlling pressurant gas temperature and controlling gas flow down on the screen (i.e., natural versus forced convection). Meanwhile, the IBP configuration is well suited to address this effect provided that careful attempts are made to heat only the gas, and not the screen. Care must also be taken to assure uniformity of temperature rise and to precisely measure the temperature of the pressurant gas before incidence on the screen. IBP configurations are preferred over IO configurations because it is better to heat the gas, then have the gas incident on the screen, rather than warm the ullagespace inside a large tank and then allow it to cool as it comes in contact with the LAD. Most discrepancies in previously reported experiments are due to these aforementioned concerns which can be mitigated through the following new experimental design.

# 7.0 Experimental Design

Testing was performed at the Cryogenic Components Lab 7 (CCL-7) at Glenn Research Center (GRC) in Cleveland, Ohio. Pore sizes for 325×2300, 450×2750, and 510×3600 Dutch Twill were determined in room temperature tests (Refs. 11 and 12). These samples were used here for heated pressurant gas tests. LAD screen samples, 6.5 cm (2.5 in.) in diameter, were cut and welded to a heavy flange to create a tight seal along the edges as shown in Figure 10. Each screen was mounted to its own flange to permit rapid change out. The screen was mated with a cylindrical cup shown in Figure 11. The purpose of the cup was to create the liquid/vapor interface (L/V) within the screen pores by pressurizing from beneath the screen for the IBP test configuration. The cup was equipped with a central support rod as shown in Figure 12. The rod had a custom fabricated cross to allow for slow, uniform pressurant gas injection into the cup. The rod also supported three donut style thin film Kapton heaters which warmed the incoming pressurant gas to the desired temperature before incidence on the LAD screen. A heater was placed on the underside of the bottom and top disc, and the top of the bottom disc, which eliminated view factors between heating source and LAD screen, and ensured that all of the heating was via conduction and convection of the incoming pressurant gas. This design forced uniform heating and pressure rise within the cup. It also eliminated direct gas impingement on the screen. Bubble point pressure was deduced from the raw differential pressure transducer (DPT) measurement from the sense line shown in Figure 11. The sensing port pointed away from the screen to eliminate flooding of the line and to eliminate two phase DPT signals. The complete assembled LAD screen and cup are shown in Figure 13.

The LAD screen and cup assembly was placed in a dewar. A polished aluminum plate was mounted to the top of the screen and cup assembly and reflected an image of the LAD screen through a viewport on the side of the dewar to camera. A fiber optic light source illuminated the screen. The purpose of the dewar was to house the liquid cryogen on top of the LAD screen. A camera was attached to the side viewport to monitor the test in real time. Time synchronization between camera and data was maintained through a custom time synchronization system. Facility air ejectors were used to control pressure and thus temperature of the liquid. The facility was modified to use GHe and $GH_2$ as pressurants for $LH_2$ testing.

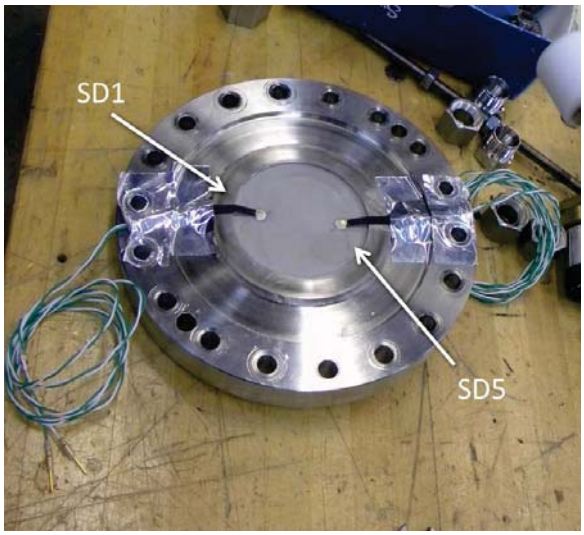

Figure 10.—LAD Screen Sample and Flange


Figure 11.—LAD Cup

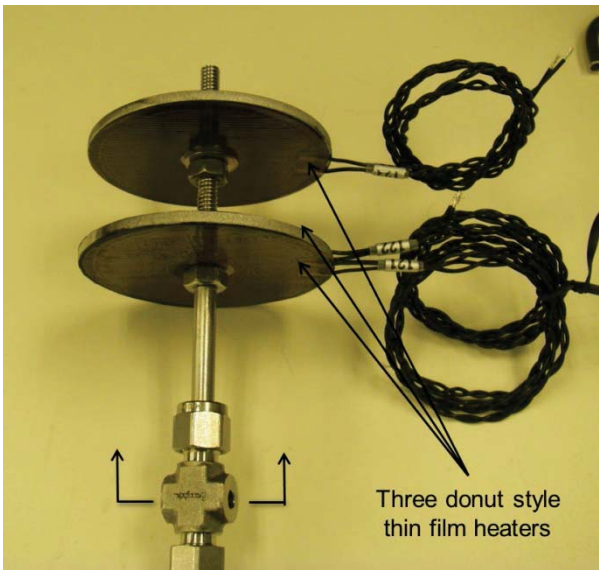

Figure 12.—Heater Bank


Figure 13.—Completed LAD Screen/Cup Assembly

Pressure in the dewar was controlled by a proportional-integral-derivative (PID) loop. Liquid temperature was controlled by conditioning the liquid in storage dewars that were connected to the facility. Liquid temperature would gradually increase due to parasitic heat leak into the dewar and through introduction of the warm pressurant gas. The liquid was evaporatively cooled by reducing pressure within the dewar. Temperature of the pressurant gas was monitored using a silicon diode inside the LAD cup and controlled by cycling on or off the heaters, which were controlled through a tight PID loop using a silicon diode inside the LAD cup.

All temperatures were measured using silicon diodes as point sensors. Critical measurements for heated pressurant gas tests here were the temperature of the liquid (SD1) and gas side (SD2) of the LAD screen, temperature of the pressurant gas (SD3 and SD4), pressure of the ullage, DPT across the LAD screen, and pressurant gas mass flow rates into the cup. All data was recorded at 5 Hz with a computer data acquisition system (DAQ). Videos of the LAD screens were time stamped and recorded to compare with the time stamp in the data. All diodes measured temperature to within 0.1 K. Ullage pressure was measured to within 2.3 kPa accuracy. The raw DPT reading was accurate to within 0.324 Pa, but due to signal interpretation and processing, read off errors, interpolation between recorded values, the total uncertainty in the corrected bubble point pressure is estimated to be 12 Pa, which is 10 percent uncertainty in the lowest reported bubble point pressure for the heated gas runs. This low absolute error in

measurement relative to previously reported cold gas tests was made possible by modifications in the DAQ system.

Experimental methodology and the original test matrix are outlined in (Ref. 16). To conduct a heated pressurant gas bubble point test, a GHe flow was first established across the screen during liquid fill of the dewar to prevent flooding of the cup. Heated pressurant gas testing here was always conducted in above atmospheric pressure conditions, which eliminated the need to pre-condition the liquid. The liquid temperature was generally fixed between a range of 20.5 to 21.0 K to allow independent examination of the effect of heated pressurant gas on LAD performance. When the dewar was filled to the desired liquid level, the pressurant gas type was selected and allowed to flow through the flow network for a period of 10 minutes or more. The screen was then allowed to reseal. The heaters were then engaged until the desired temperature of the pressurant gas was achieved. The gas was always allowed several minutes residence time to come to equilibrium at the desired gas temperature before attempting a controlled breakthrough. Then the pressure underneath the LAD screen was slowly increased until a bubble broke through the wetted screen as indicated on the live video and in the sharp rise in the DPT signal. Then the screen was resealed. Bubble points were repeated at similar pressurant gas temperatures for repeatability before moving on to the next gas temperature. Due to the low surface tension of $LH_2$ and low baseline cold gas bubble point values, it was sometimes difficult during testing to even reseal the screens. Raw bubble point pressures were corrected for liquid head pressure:

$$\Delta P_{BP}\left(T,P\right)\Big|_{\exp} = DPT - \rho_{LH2} gLL \tag{3}$$

where *LL* is the liquid level above the screen in the dewar as determined by a vertical silicon diode rake.

The test matrix consisted of the following: Three fine mesh screen channel LAD samples (325×2300, 450×2750, and 510×3600) were tested in two cryogenic liquids ($LH_2$ and $LN_2$), with two pressurization schemes (autogenous $GH_2/LH_2$) at several different pressurant gas temperatures. Bubble point data was first collected using cold pressurant gases. The cold baseline temperature was approximately equal to the liquid temperature to minimize the temperature gradient across the screen at breakdown. This was only possible because the LAD cup was immersed in the liquid. To collect data at elevated temperatures, the heaters were engaged to several different fixed gas temperatures and measurements repeated to allow comparison with the cold gas data using Equation (2).

# 8.0 Liquid Hydrogen Tests

Using the current hardware and test configuration, parametric testing was conducted to independently examine the effect of six different parameters on the bubble point pressure. The parameters included screen weave, liquid (surface tension), liquid temperature and pressure, pressurant gas type, and pressurant gas temperature. Results from testing with cold gas from (Ref. 13) are used to establish the baseline reference bubble point values. Bubble point is directly proportional to the surface tension of the liquid in Equation (1). The pressure dependence on bubble point is believed to be a modification of the temperature dependence (Ref. 19 and 20). Higher pressures relative to the saturation pressure, and thus higher levels of liquid subcooling at the screen, produced higher bubble points for previously reported LOX and $LCH_4$ data.

Figure 14 establishes the effect of changing the screen weave, liquid temperature, and pressurant gas on the $LH_2$ bubble point pressure by plotting data for all three screen meshes and both pressurant gases. The trends are as follows: First, for all three meshes, and for both pressurant gases, bubble point decreases with increasing liquid temperature, due to decreasing surface tension. The highest bubble point pressures are always obtained in the coldest liquid temperatures, regardless of screen or gas type. Second, for all three meshes, regardless of liquid temperature, bubble points obtained using the noncondensible gas are always higher than those obtained using the condensable gas. Gaseous helium adds margin to the bubble point pressure while $GH_2$ acts like a degradation factor. The disparity between pressurization schemes is relatively fixed for all three LAD screen meshes tested here. Third, for all liquid temperatures and for both pressurant gases, bubble point pressure does not scale with the mesh of the screen. This is the most complex trend of the original five parameters tested in (Ref. 14). The second finest 450×2750 mesh produced the highest bubble points, for both GHe and $GH_2$. The 510×3600 mesh outperforms the 325×2300 mesh at $LH_2$ temperatures, but the 325×2300 yielded higher pressures in room temperature liquids (Refs. 11 and 12). The reason for this crossover in performance is due to the temperature dependence of the screen pore diameter, as mentioned previously. In addition, the controlling parameter for gain in performance with reduced temperature is the shute to warp diameter ratio. The geometry of the L/V interface at breakthrough is dependent on this ratio, and as previously shown, the 510 screen has the largest gain at $LH_2$ temperatures.

The sixth and final parameter that was investigated was the temperature of the pressurant gas. Data is first presented on an absolute scale to allow direct comparison to cold gas data. Figure 15 plots all $LH_2$ bubble point data collected using warm pressurant gas. Data is plotted as a function of the temperature difference between warm gas and cold liquid at breakthrough. Controlled breakthroughs and reseals were achieved for gas temperatures between 30 K < $T_{GAS}$ < 116 K which correspond to a temperature difference across the screen of 10 K < $\Delta T$ < 95 K. As shown for all three screens, the bubble point pressure decreases linearly with increasing

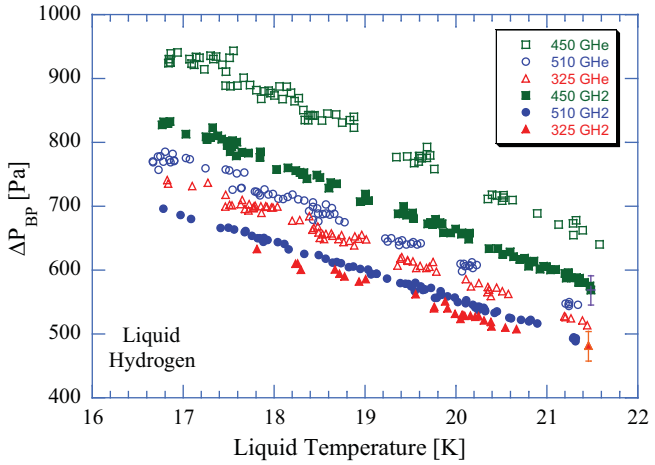


Figure 14.—Cold Gas Liquid Hydrogen Bubble Point as a Function of Liquid Screen Side Temperature

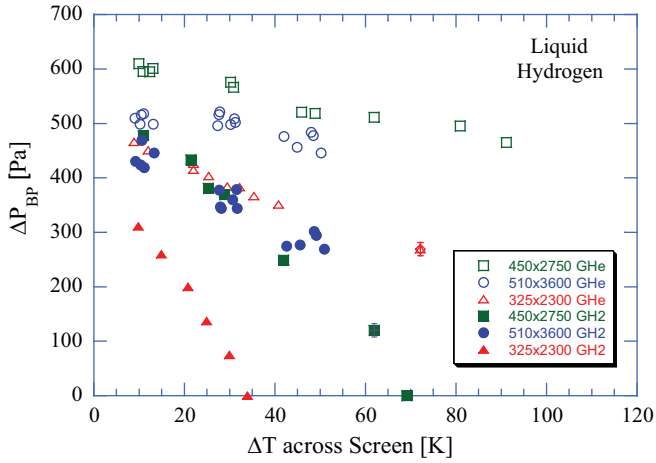


Figure 15.—Heated Pressurant Gas $LH_2$ Bubble Point as a Function of Temperature Difference across the Screen.

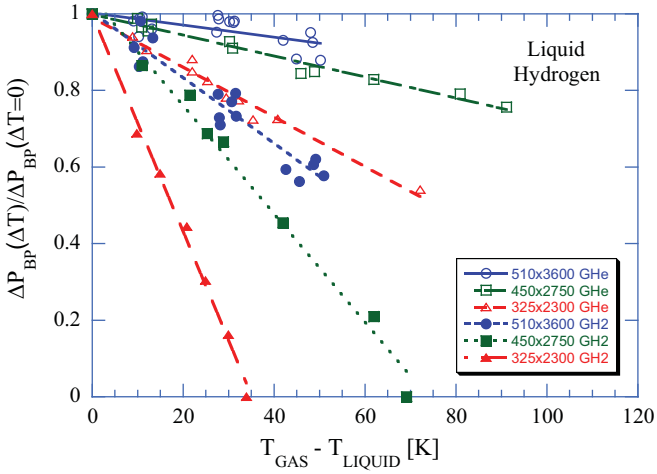


Figure 16.—Normalized Heated Pressurant Gas $LH_2$ Bubble Point Pressure as a Function of the Temperature Difference between Pressurant Gas and Liquid at the LAD Screen.

pressurant gas temperature. The degradation in bubble point is more pronounced using $GH_2$ versus pressurizing with GHe as the 325×2300 and 450×2750 screens failed to reseal at temperature differences of 34 and 69 K, respectively using the condensable gas. Meanwhile, controlled breakthroughs were achieved with all three meshes using GHe beyond temperature differences of 50 K. Regardless of the gas type, the onset of degradation is immediate for gas temperatures greater than the liquid temperature. This is in contrast to previously reported $LH_2$ heated gas bubble point pressures where the onset of degradation would occur at a certain gas temperature.

Figure 16 plots heated bubble point pressures using Equation (2) to normalize the data to the cold gas value obtained at the liquid temperature. Since each controlled breakthrough/reseal pair occurred at different liquid temperatures spaced over an approximate temperature range of 20.5 K < $T$ < 21.1 K, each point was normalized to its own cold gas bubble point pressure, as opposed to a single value. Therefore, at a temperature difference across the screen of 0 K, there is no deviation from the unheated pressurant gas bubble point ratio, by definition. Data is again plotted as a function of the $\Delta T$ across the screen. Lines are simple linear fits to the data.

Normalizing the data shows three distinct trends. First, for all three screens and both pressurant gases, heating the gas above the liquid temperature acts as a degradation factor on the cold gas bubble point pressure. The larger the temperature difference across the screen, the earlier the screen will break down. Second, for all three screens, as also indicated in Figure 15, bubble point pressure degrades from the cold gas value much more rapidly using condensable gas than using noncondensible gas as indicated by steeper slopes in the linear curve fits. Third, for both pressurization schemes, degradation in bubble point is inversely proportional to the porosity of the screen. Porosity is the ratio of open area for fluid to flow through the screen divided by the total screen area. Porosity for the LAD screens is defined as:

$$\varepsilon = 1 - \frac{\pi}{4}\left(n_w d_w^2 + 0.5 n_s d_s^2 + 0.5 n_w n_s d_s^2 l_s\right) \tag{4}$$

where $n_w$ and $n_s$ are the number of warp and shute wires per inch of screen material, respectively, $d_w$ and $d_s$ are the diameters of the warp and shute wires, and $l_s$ is the distance between consecutive shute wires as defined as (Ref. 30):

$$l_s = \sqrt{\left(d_w + d_s\right)^2 + \left(\frac{1}{n_w}\right)^2} \tag{5}$$

Computed screen thicknesses and porosities are shown in Table 1. Therefore higher porosities indicate more open area for the gas to interact directly with the liquid. As shown in Figure 16, the finest 510×3600 mesh exhibited the smallest degradation in performance over the 450×2750 and 325×2300

screen, as indicated by the slopes of the linear curve fits. This trend holds for both pressurization schemes. As is evident in Figure 15 and Figure 16, although the 450×2750 screen outperforms the 510×3600 on an absolute basis, degradation in performance for the 510×3600 screen is less.

TABLE I.—CALCULATED SCREEN PARAMETERS

| Screen | Screen thickness, μm | $l_s$, μm | ε |
|---|---|---|---|
| 325×2300 | 88.9 | 100.7 | 0.245 |
| 450×2750 | 66 | 72.8 | 0.267 |
| 510×3600 | 56.4 | 65.0 | 0.284 |

Coarser screens are likely to build up higher temperature differences across the screen prior to bubble breakthrough, causing the local interfacial temperature to increase significantly higher than finer meshes. For Dutch Twill screens, the screen thickness for a heated gas bubble to traverse from gas to liquid side of the screen is approximately equal to (Ref. 30):

$$t = \left(2 * d_{\text{shute}}\right) + d_{\text{warp}} \tag{6}$$

Therefore coarser Dutch Twills are thicker and have lower porosities relative to finer Dutch Twills. These longer path lengths for warm gas or vapor to travel through the screen coupled with less overall open volume for gas and liquid to exchange heat and mass causes larger temperature differences to build across the screen before the actual visible warm gas bubble breaks through the screen. The finest 510 mesh is the thinnest screen and has the smallest pores, and largest porosity, making it easier for heat and mass to transport across the screen between liquid and gas prior to breakdown. Since mass is more easily transferrable across the screen, the local gas at the screen pore will cool slightly, cooling the interface temperature relative to the coarser meshes long before the bubble breaks through the screen. Meanwhile, for the coarser mesh, the larger pore size, thicker screen, and lower porosity causes larger temperature differences across the screen to build prior to breakdown. The larger pore sizes and less contact area between warm gas and cold liquid prevent heat transfer from the gas into the liquid.

Coarser screens like 200×1400 and 325×2300 act more like an insulator resulting in large temperature differences across the screen (Ref. 31). The dominate mode of heat transfer for the finer mesh screens is primarily parallel path heat conduction: conduction within the metal and conduction within the liquid phase trapped initially in the mesh. Except at breakthrough, there is no convective motion through the screen as the tiny pore size and the liquid viscosity limit the motion.

The degradation in performance using condensable gas can also be explained as follows: As warm condensable vapor passes through the screen, it condenses into the liquid, and warms the L/V interface, reducing the surface tension and thus bubble point. For GHe pressurization, the small additional margin in bubble point pressure is due to the suppression of the local partial pressure of $GH_2$ within the screen pores. Free mass transport is minimized with helium present, but heat conduction between warm gas and cold liquid still occurs at a slightly lower rate relative to $GH_2$ pressurization. Messerole and Jones (Ref. 29) speculated that for $GH_2$ pressurization, the liquid may be in a locally superheated state at the screen, which may cause any heat input into the liquid to produce bubbles immediately and lead to the liquid detaching from the screen. Meanwhile, for GHe pressurization, the liquid at the screen may be in a slightly subcooled state, since GHe has been shown to evaporate liquid away from the screen (Refs. 19 and 20).

Results are in fair agreement with Cady's (Ref. 26) previously reported NIBP results using a 325×2300 mesh and GHe; he showed a smaller degradation factor (despite higher heat transfer rates) of only 10 percent at a gas temperature 55 K above the liquid temperature. However, Cady also reports near identical degradation in performance for several different meshes, which is in disagreement with the current study. The current study is also in agreement with Burge and Blackmon's (Ref. 7) heated $GH_2$ NIBP data for a 250×1370 that showed steeper degradation relative to the 325×2300 $GH_2$ here. Note that the 250×1370 screen has a lower porosity relative to the 325×2300 and would be expected to degrade more relative to the finer meshes.

# 9.0 Conclusion

Experimental results here confirm that elevating the pressurant gas temperature above the liquid temperature always acts as a degradation factor on the performance of the LAD. Three fine mesh screen channel LAD samples were tested in $LH_2$ using heated noncondensible (GHe) and condensable ($GH_2$/$LH_2$) gases for temperature difference between the pressurant and liquid of 0 to 91K for $LH_2$. For all three meshes, both liquids, and both pressurization schemes, normalized bubble point pressure ratio decreases linearly with increasing gas temperatures. Degradation in performance is much sharper using condensable gases versus using noncondensible gases. The reduction in LAD performance scales inversely with the porosity of the screen for both liquids and pressurization schemes, as the finest 510×3600 screen exhibited the least amount of degradation, and the coarsest 325×2300 had the highest reduction in performance. For heated $LH_2$ bubble point tests, the onset of degradation always occurred immediately with warm gas for all three meshes. Differences in performance between the three different screens are due to the effect of the screen thickness and porosity on the overall heat transfer across the LAD screen. Differences in performance

between pressurants are due to modified heat and mass transport at the screen pore L/V interface through evaporation (GHe) and/or condensation ($GH_2$).

Results here have direct impact on future LAD and pressurization system design for low surface tension liquids, especially the CPST TDM and future cryogenic hydrogen fueled depots. The bubble point pressure of screen channel liquid acquisition devices represents the upper limit on the total allowable pressure loss, and thus flow rate from the LAD to a transfer line en route to an engine or receiver depot tank. Higher bubble points are always obtained when the gas used to pressurize the propellant tank, and thus flow liquid through the LAD, is as cold as possible relative to the liquid, with the highest values obtained when the pressurant gas and liquid temperature are approximately equal. However, unless the pressurant gas bottles and propellant tanks are thermally linked, or subsurface pressurization methods are employed, the gas will always be significantly warmer than the cryogenic propellant and some degradation in LAD performance will be expected for all real mission scenarios. This work quantifies this effect.

# References


1. McLean, C., Mustafi, S., Walls, L., Pitchford, B., Wollen, M., and Schmidt (2011) "Simple, Robust Cryogenic Propellant Depot for Near Term Applications," 2011 IEEE Aerospace Conference, Big Sky, MT.
2. Fester, D.A., Villars, A.J., and Uney, P.E. (1975) "Surface Tension Propellant Acquisition System Technology for Space Shuttle Reaction Control Tanks," AIAA-75-1196 11th AIAA/SAE Propulsion Conference, Anaheim, CA, Sep. 29 – Oct. 1, 1975.
3. Peterson, R. and Uney, P. (1978) "Development and Qualification of the Space Shuttle Orbiter Reaction Control System Propellant Tank," AIAA-78-1026 AIAA/SAE 14th Joint Propulsion Conference, Las Vegas, NV, Jul. 25–27 1978.
4. Schweickert, T.F. (1981) "Design of the Aft Propulsion Subsystem for Long Life," JANNAF Propulsion Meeting, New Orleans, LA, May 26–28, 1981.
5. Anglim, D.D. (1981) "Space Shuttle Aft Propulsion Subsystem" AIAA-81-1511.
6. Anderson, J.E. (1989) "Superfluid Helium Acquisition System Development," Cryogenics 29, 513–516.
7. Burge, G.W. and Blackmon, J.B. (1973) "Study and Design of Cryogenic Propellant Acquisition Systems – Volume II – Supporting Experimental Program," NAS8-27685 MDAC Report MDC G5038.
8. Burge, G.W., Blackmon, J.B., and Castle, J.N. (1973) "Design of Propellant Acquisition Systems for Advanced Cryogenic Space Propulsion Systems," AIAA/SAE Propulsion Conference Las Vegas, NV, Nov. 5–7, 1973.
9. Zimmerli, G.A., Asipauskas, M., Van Dresar, N.T. (2010) "Empirical Correlations for the Solubility of Pressurant Gases in Cryogenic Propellants" Cryogenics 50, 556–560.
10. Stiegemeier, B., Williams, G., Melcher, J.C., and Robinson, J. (2010) "Altitude Testing of an Ascent Stage LOX/Methane Main Engine," 5th JANNAF Liquid Propulsion Subcommittee Meeting, May 2010.
11. Hartwig, J.W., and Mann, J.A. (2012 I) "A Simplified Model for Predicting the Breakdown Point of Screen Channel Liquid Acquisition Devices," AiCh Journal (accepted for publication).
12. Hartwig, J.W., and Mann, J.A. (2012 II) "Bubble Point Pressures of Binary Methanol/Water Mixtures," AICHe Journal (accepted for publication).
13. Hartwig, J.W., Darr, S.R., and Mann, J.A. (2013) "Parametric Analysis on the Liquid Hydrogen Bubble Point," AICHe Journal (in press).
14. Hartwig, J.W., McQuillen, J.B., and Chato, D.J. (2013) "Screen Channel LAD Bubble Point Tests in Liquid Hydrogen," AIChE Journal (in press).
15. Jurns, J.M. and McQuillen, J.B. (2008) "Liquid Acquisition Device Testing with Sub-cooled Liquid Oxygen," AIAA-2008-4943 44th Joint Propulsion Conference and Exhibit, Hartford, CT, Jul. 21–23, 2008.
16. Hartwig, J.W., McQuillen, J.B., and Chato, D.J. (2013) "Performance Gains of Propellant Management Devices for Liquid Hydrogen Depots," 51st Aerospace Sciences Meeting, Grapevine, TX, Jan. 7–11, 2013.
17. Hartwig, J.W. and McQuillen, J. (2011) "Analysis of Screen Channel LAD Bubble Point Tests in Liquid Oxygen at Elevated Temperature," 41nd AIAA Thermophysics Conference, Honolulu, HI, Jun. 27–30, 2011.
18. Hartwig, J.W. and McQuillen, J. (2011) "Analysis of Screen Channel LAD Bubble Point Tests in Liquid Methane at Elevated Temperature" 50th Aerospace Sciences Meeting, Nashville, TN, Jan. 9–12, 2012.
19. Hartwig, J.W., McQuillen, J., and Jurns, J. (2012) "Screen Channel LAD Bubble Point Tests in Liquid Oxygen," Journal of Thermophysics and Heat Transfer (in press).
20. Hartwig, J.W. and McQuillen, J. (2012) "Screen Channel LAD Bubble Point Tests in Liquid Methane," Journal of Thermophysics and Heat Transfer (in press).
21. Castle, J.N. and Klevatt, P.L. (1972) "Heat Transfer Effects on Bubble Point Tests in Liquid Nitrogen," MDC02653.
22. Paynter, H.L. and Page, G.R. (1973) "Acquisition/Expulsion System for Earth Orbital Propulsion System Study, Volume II," NASA-CR-134154.
23. Blackmon, J.B. (1974) "Design, Fabrication, Assembly, and Test of a Liquid Hydrogen Acquisition Subsystem," NASA CR-120447.
24. Warren, R.P. (1975) "Acquisition System Environmental Effects Study," NASA CR-120768.
25. Warren, R.P., Butz, J.R., and Maytum, C.D. (1975) "Measurements of Capillary System Degradation," AIAA-75-1197.

26. Cady, E.C., (1975) “Design and Evaluation of Thermodynamic Vent/Screen Baffle Cryogenic Storage System,” NASA CR-134810.
27. Wilson, A.C. and Messerole, J.S. (1986) “Liquid Hydrogen Acquisition Device Component Fabrication and Testing,” D180-29345-1.
28. Bennett, F.O. (1987) “Design and Demonstrate the Performance of Cryogenic Components Representative of Space Vehicles, Start Basket Liquid Acquisition Device Performance Analysis,” NASA CR-179138.
29. Messerole, J.S. and Jones, O.S. (1993) “Pressurant Effects on Cryogenic Liquid Acquisition Devices,” Journal of Spacecraft and Rockets 30, 236–243.
30. Armour, J. and Cannon, J. (1968) “Fluid Flow through Woven Screens,” AICHe Journal, 14, 415–420.
31. Li, C. and Peterson, G.P. (2006) “The Effective Thermal Conductivity of Wire Screen,” International Journal of Heat and Mass Transfer 49, 4095–4105.